Influence of chemically radiative hydrodynamic Casson flow over an exponentially slandering surface with heat generation

M. Gayatri[1], Kalyani Cherukuru[2], B. Sarath Babu[3], K. Subhashini[4]
[1]Associate Professor, Department of Mathematics, Geethanjali Institute of Science and Technology, Nellore, A.P, India
[2]Professor, Department of Mathematics, Viswam Engineering College, Madanapalli, A.P, India.
[3]Professor, Department of Mathematics, Siddharth Institute of Engineering & Technology, Puttur, Tirupathi-Dist. A.P, India
[4]Associate Professor, Siddharth Institute of Engineering & Technology, Puttur, Tirupathi-Dist. A.P, India

Abstract
A boundary value problem is addressed in this paper which models a two-dimensional electrically conducting Casson nanofluid over an exponentially slendering surface with variable thickness. The flow area takes into account the effects of thermal radiation, heat source, Brownian motion, thermophoretic diffusion and chemical reaction. To get the ordinary differential equations from the governing partial differential equations, a suitable similarity transformation is used. The homotopy analysis method (HAM) is used to solve these equations as well as the boundary conditions. Effects of magnetic parameter (M), Casson parameter (β), velocity power index parameter (m), Brownian motion parameter (Nb), thermophoresis parameter (Nt), radiation parameter (R), heat source parameter (Q), Prandtl number (Pr), Schmidt number (Sc) and chemical reaction (γ)on velocity, temperature, concentration, friction factor, local Nusselt number and local Sherwood number are given using graphs and tables for $\chi = 0.0$ (exponentially stretching sheet) and $\chi \neq 0.0$ (exponentially slendering sheet). As compared to the flow over an exponentially slendering sheet, the flow over an exponentially stretching sheet has a greater effect on heat transfer rate.

Keywords: Casson nanofluid, thermal radiation, variable thickness, exponentially slendering sheet, HAM.
How to cite this article: Gayatri M, Cherukuru K, Sarath Babu B, Subhashini K. Influence of Chemically Radiative Hydrodynamic Casson Flow Over an Exponentially Slandering Surface with Heat Generation. Int J Drug Deliv Technol. 2026;16(72s): 1717-1729. DOI: 10.25258/ijddt.16.72s.193

Nomenclature

$x,\ y$	directions along and normal to the surface	q_w	surface heat flux
u, v	velocity components in $x,\ y$ directions	$\chi = A\sqrt{\dfrac{(m+1)U_0}{2\nu L}}$	wall thickness parameter
$B = B_0\, e^{\frac{x}{2L}}$	magnetic field	Nu_x	local Nusselt number
T	temperature of the fluid	Sh_x	local Sherwood number
k	thermal conductivity	$Q = \dfrac{2LQ_0}{\rho C_p U_w}$	heat source parameter
C_p	specific heat at constant pressure	$Sc = \dfrac{\nu}{D_B}$	Schmidt number
D_B	Brownian diffusion coefficient	Re_x	local Reynolds number
C	nanoparticle volume fraction	*Greek symbols*	
D_T	Thermophoretic diffusion coefficient	ν	kinematic viscosity
T_∞	ambient temperature	ρ	fluid density
Q_0	heat source coefficient	σ	Electrical conductivity
C_∞	ambient nanoparticle volume	τ	ratio between the effective

	fraction		heat capacity of the nanoparticle material and heat capacity of the fluid
U_0	reference velocity	ψ	stream function
$U_w = U_0\, e^{\frac{x}{L}}$	stretching velocity	η, ξ	similarity variables
$T_w(x)$	temperature at the surface	θ	dimensionless temperature in $[\chi, \infty)$
$C_w(x)$	nanoparticle concentration at the surface	Θ	dimensionless temperature with respect to $[0, \infty)$
A	coefficient related to exponentially stretching sheet	ϕ	dimensionless nanoparticle volume fraction in $[\chi, \infty)$
f	dimensionless stream function in $[\chi, \infty)$	Φ	dimensionless nanoparticle volume fraction with respect to $[0, \infty)$
F'	dimensionless fluid velocity with respect to $[0, \infty)$	μ	dynamic viscosity
L	reference length	μ_∞	ambient dynamic viscosity
m	velocity power index parameter	τ_w	wall shear stress
$M = \dfrac{2\sigma B_0^2}{\rho U_0}$	Magnetic parameter	j_w	surface mass flux
$Pr = \dfrac{\rho C_p}{\nu}$	Prandtl number	σ^*	Stefan-Boltzman constant
$Nb = \dfrac{\tau D_B (C - C_\infty)}{\nu}$	Brownian motion parameter	k^*	mean absorption coefficient
$Nt = \dfrac{\tau D_T (T - T_\infty)}{\nu T_\infty}$	thermophoresis parameter	*Subscripts*	
q_r	radiative heat flux	w	condition at the surface
β	Casson parameter	∞	condition at the free stream
$R = \dfrac{4\sigma^* T_\infty^3}{k^* k}$	radiation parameter		
$\gamma = \dfrac{2k_0 L}{U_w}$	chemical reaction parameter		

Introduction

Great attention has been carried out in the direction of non-Newtonian fluids in view of their encouraging applicability in various branches of engineering and technology like in the processing of polymers, biomechanics, enhanced oil recovery, food products, etc. Rajagopal [1, 2] made some impressive research on differential type fluids. Siddiqui and Kaloni [3] and Hayat et al. [4] studied the nature of second grade fluid. Vieru et al. [5] obtained some exact solutions for the flow of an Oldyord-B fluid due to an infinite flat plate. Aliakbar et al. [6] studied the effect of uniform magnetic field on Maxwellian fluid under thermal radiation. Hayat and Kara [7] obtained the analytical solution for the third grade fluid flow by considering a magnetic field of variable strength. Nandeppanavar et al. [8] analyzed the viscoelastic fluid flow with non uniform heat source/sink and thermal radiation. Sahoo [9] reported the flow and heat transfer properties of a third grade fluid subject to partial slip. Hamad [10] analyzed the flow of nanofluid in the presence magnetic field.

Owing to their robust existence and lack of other problems such as sedimentation, degradation, additional pressure drop, and so on, nanofluids have a wide range of applications in various scientific fields and industries. These fluids are used in power generators, micro production, vehicles, and other applications. Tiwari and Das [11] and Moaiga et al. [12] deduced that thermal conductivity can be increased by the introduction of nanoparticles in the fluids and hence the features of heat transfer. Sheremet [13] obtained the numerical solutions for the free convection flow of nanofluid under thermal stratification. Das et al. [14] discussed the boundary layer slip flow and heat transfer of nanofluid over a stretching sheet. Mabood et al. [15] reported the properties of nanofluid flow over a nonlinear stretching sheet. Shehzad et al. [16] have taken the convective mass condition and analyzed the MHD boundary layer flow on nanofluid. Ramana Reddy et al. [17] observed the higher heat transfer rate in Ag-water when compared with TiO_2-water nanofluid.

Many researchers have allured the concept of Casson fluid as they have many applications in the fields like polymer processing, biomechanics, drilling operations, metallurgy, etc. Casson fluid constitutive equation delineate a nonlinear relationship among stress and rate of strain and has been observed to be perfectly admissible to silicon suspensions, suspensions of bentonite in water, and lithographic varnishes used for printing inks. Mukhopadhyay [18] reported that the Casson parameter depreciates the velocity field. Pramanik [19] observed the behaviour of Casson fluid flow over an exponentially porous stretching surface. Nadeem et al. [20] studied the MHD three dimensional Casson fluid flow over a linear stretching sheet. Ibrahim et al. [21] analyzed the mixed convection flow of Casson nanofluid with chemical reaction and heat source. The magnetohydrodynamic (MHD) stagnation point flow of Casson nanofluid over a nonlinear stretching sheet in the presence of velocity slip and convective boundary condition is studied by Ibrahim et al. [22].

In this article, we consider a stretching with variable thickness. This type of sheet is generally used in machine design, nuclear reactor technology, architecture, acoustical components, naval structures, etc. Lee [23] initiated the idea of variable thickness sheet. Fang et al. [24] extended this problem to study the boundary layer flow. Khader and Megahed [25, 26] discussed the flow analysis over a variable thickness stretching sheet by taking slip velocity in to consideration.

Here we analyze the MHD flow over an exponentially slendering sheet with thermal radiation, chemical reaction and heat source. In the mathematical model Brownian motion and thermophoretic diffusion of nanoparticles are considered. The obtained model was solved by HAM. It has been proved that this technique is a worthful approach in dealing with various problems [27-30].

Mathematical formulation

Consider a steady two-dimensional MHD Casson nanofluid flowing over an exponentially slendering stretching layer of variable thickness. Thermal radiation, heat source, and chemical reaction are all taken into account. The combined effect of Brownian motion and thermophoresis was also considered. The stretching velocity at the free stream is of the form $U_w = U_0\, e^{\frac{x}{L}}$. The Casson fluid flow is assumed to occupy the domain $A e^{-\frac{x}{2L}} \le y < \infty$ as shown in the Fig. 1. It is also assumed that a magnetic field of strength $B = B_0 e^{\frac{x}{2L}}$ is applied perpendicular to the Casson nanofluid flow. T_w and C_w are taken as the wall temperature and nanoparticle concentration, T_∞ and C_∞ are the ambient values of temperature and nanoparticle concentration.

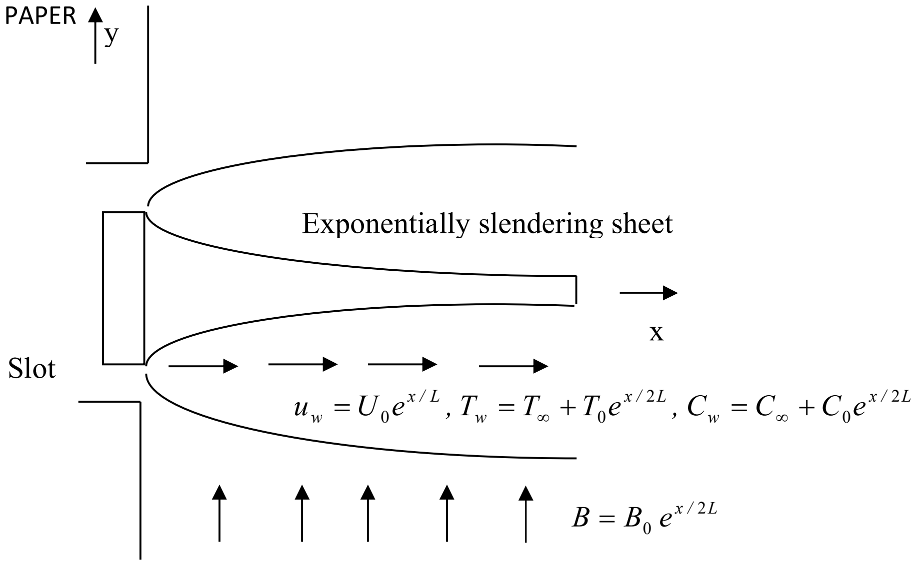

Fig. 1. Coordinate system of the Casson nanofluid flow.

The rheological equation of state for an isotropic and incompressible flow of a Casson fluid is

$$\tau_{ij} = \begin{bmatrix} 2\left(\mu_B + \dfrac{p_y}{\sqrt{2\pi}}\right)e_{ij}, & \pi > \pi_c \\ 2\left(\mu_B + \dfrac{p_y}{\sqrt{2\pi_c}}\right)e_{ij}, & \pi_c > \pi \end{bmatrix},$$

where μ_B is the dynamic viscosity of the non-Newtonian fluid, p_y is the yield stress of the fluid, π is the product of the component of deformation rate with itself, $\pi = e_{ij}e_{ij}$, e_{ij} is the $(i,j)^{th}$ component of the deformation rate and π_c is the critical value of this product based on the non-Newtonian model. Under the boundary layer approximations, the governing equations for of this problem can be expressed as

$$\frac{\partial u}{\partial x} + \frac{\partial v}{\partial y} = 0, \qquad (1)$$

$$u\frac{\partial u}{\partial x} + v\frac{\partial u}{\partial y} = \nu\left(1+\frac{1}{\beta}\right)\frac{\partial^2 u}{\partial y^2} - \frac{\sigma B(x)^2}{\rho}u, \qquad (2)$$

$$u\frac{\partial T}{\partial x} + v\frac{\partial T}{\partial y} = \frac{k}{\rho C_p}\frac{\partial^2 T}{\partial y^2} - \frac{1}{\rho C_p}\frac{\partial q_r}{\partial y} + \tau\left[D_B\left(\frac{\partial C}{\partial y}\frac{\partial T}{\partial y}\right) + \frac{D_T}{T_\infty}\left(\frac{\partial T}{\partial y}\right)^2\right] + \frac{Q_0}{\rho C_p}(T-T_\infty), \qquad (3)$$

$$u\frac{\partial C}{\partial x} + v\frac{\partial C}{\partial y} = D_B\left(\frac{\partial^2 C}{\partial y^2}\right) + \frac{D_T}{T_\infty}\left(\frac{\partial^2 T}{\partial y^2}\right) - k_0\left(C - C_\infty\right). \qquad (4)$$

The boundary conditions are

$$\begin{aligned} &u = U_w,\ \ v = 0,\ \ T = T_w,\ \ C = C_w \ \ at \ \ y = Ae^{-\frac{x}{2L}}, \\ &u = 0, \qquad\qquad T = T_\infty,\ \ C = C_\infty,\ \ at \ \ y = \infty. \end{aligned} \qquad (5)$$

By using Rosseland approximation, we have

$$q_r = -\frac{4\sigma^*}{3k^*}\frac{\partial T^4}{\partial y}.$$

Taylor's series is utilized in taking the following expression

$$\mathrm{T}^4 \cong 4T_\infty^3 T - 3T_\infty^4.$$

We assume that the surface is retained at a temperature and nanoparticle volume fraction

$$T_w = T_\infty + T_0 e^{\frac{x}{2L}}\theta(\eta),\ C_w = C_\infty + C_0 e^{\frac{x}{2L}}\phi(\eta).$$

Now we induce the similarity transformations

$$\psi(x,y) = f(\eta)\sqrt{\frac{2\nu U_0 L}{m+1}}e^{\frac{x}{2L}},\ \eta = e^{\frac{x}{2L}}\sqrt{\frac{(m+1)U_0}{2\nu L}}y, T = T_\infty + (T_w - T_\infty)\theta(\eta),$$

$$C = C_\infty + (C_w - C_\infty)\phi(\eta), u = \frac{\partial\psi}{\partial x} = U_0 f'(\eta)e^{\frac{x}{L}},$$

$$v = -\frac{\partial\psi}{\partial y} = -\sqrt{\frac{\nu U_0}{2L(m+1)}}e^{\frac{x}{2L}}\left(f(\eta) + \eta f'(\eta)\right) \qquad (6)$$

Here u and v satisfy the continuity equation. Equations (2) to (5) become

$$\left(1+\frac{1}{\beta}\right)f'''+\left(\frac{1}{m+1}\right)\left[f\,f''-2(f')^2-M\,f'\right]=0, \quad (7)$$

$$\left(1+\frac{4R}{3}\right)\theta''+Pr\left[\frac{1}{m+1}(f\theta'-f'\theta+Q\theta)+Nb\theta'\phi'+Nt\theta'^2\right]=0 \quad (8)$$

$$\phi''+\frac{Nt}{Nb}\theta''+\frac{Sc}{m+1}(f\phi'-f'\phi-\gamma\phi)=0. \quad (9)$$

The boundary conditions are

$$f(\chi)=-\chi,\ f'(\chi)=1,\quad \theta(\chi)=1,\quad \phi(\chi)=1,$$
$$f'(\infty)=0,\qquad \theta(\infty)=0,\qquad \phi(\infty)=0. \quad (10)$$

To execute the calculations easily, we avail the functions $F(\zeta)=F(\eta-\chi)=f(\eta)$, $\Theta(\zeta)=\Theta(\eta-\chi)=\theta(\eta)$ and $\Phi(\zeta)=\Phi(\eta-\chi)=\varphi(\eta)$. Then the above equations take the form

$$\left(1+\frac{1}{\beta}\right)F'''+\left(\frac{1}{m+1}\right)\left[F\,F''-2(F')^2-M\,F'\right]=0, \quad (11)$$

$$\left(1+\frac{4R}{3}\right)\Theta''+Pr\left[\frac{1}{m+1}(F\Theta'-F'\Theta+Q\Theta)+Nb\Theta'\Phi'+Nt\Theta'^2\right]=0, \quad (12)$$

$$\Phi''+\frac{Nt}{Nb}\Theta''+\frac{Sc}{m+1}(F\Phi'-F'\Phi-\gamma\Phi)=0. \quad (13)$$

The boundary conditions are

$$F(0)=-\chi,\ F'(0)=1,\quad \Theta(0)=1,\ \Phi(0)=1,$$
$$F'(\infty)=0,\qquad \Theta(\infty)=0,\qquad \Phi(\infty)=0. \quad (14)$$

In nanofluid problems, the physical quantities of interest are friction factor (C_f), wall heat transfer (Nu_x) and the volume fraction mass transfer (Sh_x) is defined as:

$$C_f=\frac{\tau_w}{\frac{1}{2}\rho U_w^2},\ Nu_x=\frac{x\,q_w}{k(T_w-T_\infty)},\ Su_x=\frac{x\,j_w}{k(C_w-C_\infty)},$$

where

$$\tau_w=\mu\left(\frac{\partial u}{\partial y}\right),\ q_w=-k\left(\frac{\partial T}{\partial y}\right)\ j_w=-D_B\left(\frac{\partial C}{\partial y}\right)$$

at $y=Ae^{-\frac{x}{2L}}$.

Using above quantities, we have

$$Re_x^{1/2}\,C_f=2\left(1+\frac{1}{\beta}\right)\sqrt{\frac{m+1}{2}}F''(0),$$

$$Re_x^{-1/2}\,Nu_x=-\left(1+\frac{4}{3}R\right)\left(\frac{x}{L}\right)\sqrt{\frac{m+1}{2}}\,\Theta'(0)$$

and

$$Re_x^{-1/2}\,Sh_x=-\left(\frac{x}{L}\right)\sqrt{\frac{m+1}{2}}\,\Phi'(0),$$

where $Re_x=\frac{U_w L}{\nu}$ is the local Reynolds number.

HAM

To build up the homotopic solutions of equations (11) to (14), we pick up the initial guesses and linear operators as follows

$$F_0(\zeta)=-\chi+1+e^{-\zeta},$$
$$\Theta_0(\zeta)=e^{-\xi\zeta},$$
$$\Phi_0(\zeta)=e^{-\zeta},$$

$$L_1(F)=F'''-F',$$
$$L_2(\Theta)=\Theta''-\Theta,$$
$$L_3(\Phi)=\Phi''-\Phi,$$

with

$$L_1\left(C_1+C_2e^{\zeta}+C_3e^{-\zeta}\right)=0,$$
$$L_2\left(C_4e^{\zeta}+C_5e^{-\zeta}\right)=0,$$
$$L_3\left(C_6e^{\zeta}+C_7e^{-\zeta}\right)=0,$$

where C_i $(i=1$ to $7)$ are the arbitrary constants.

We construct the zeroth-order deformation equations

$$(1-p)L_1\left(F(\zeta;p)-F_0(\zeta)\right)=p\hbar_1 N_1\left[F(\zeta;p)\right], \quad (15)$$

$$(1-p)L_2\left(\Theta(\xi;p)-\Theta_0(\zeta)\right)=p\hbar_2 N_2\left[F(\zeta;p),\Theta(\zeta;p),\Phi(\zeta;p)\right], \quad (16)$$

$$(1-p)L_3\left(\Phi(\xi;p)-\Phi_0(\zeta)\right)=p\hbar_3 N_3\left[F(\zeta;p),\Theta(\zeta;p),\Phi(\zeta;p)\right], \quad (17)$$

subject to the boundary conditions

$$F(0;p)=-\chi,\quad F'(0;p)=1,\quad F'(\infty;p)=0,$$
$$\Theta(0;p)=1,\quad \Theta(\infty;p)=0,$$
$$\Phi(0;p)=1,\quad \Phi(\infty;p)=0,$$

(18)

Where

$$N_1\left[F(\zeta;p)\right]=\left(1+\frac{1}{\beta}\right)\frac{\partial^3 F(\zeta;p)}{\partial\zeta^3}+\frac{1}{m+1}\left[\begin{array}{l}F(\zeta;p)\dfrac{\partial^2 F(\zeta;p)}{\partial\zeta^2}-2\left(\dfrac{\partial F(\zeta;p)}{\partial\zeta}\right)^2\\ -M\dfrac{\partial F(\zeta;p)}{\partial\zeta}\end{array}\right],$$

(19)

$$N_2\left[F(\zeta;p),\Theta(\zeta;p),\Phi(\zeta;p)\right]=\left(1+\frac{4}{3}R\right)\frac{\partial^2\Theta(\zeta;p)}{\partial\zeta^2}$$
$$+\Pr\left(\begin{array}{l}\dfrac{1}{m+1}\left(F(\zeta;p)\dfrac{\partial\Theta(\zeta;p)}{\partial\zeta}-\dfrac{\partial F(\zeta;p)}{\partial\zeta}\Theta(\zeta;p)+Q\Theta(\zeta;p)\right)\\ +\left(Nb\dfrac{\partial\Theta(\zeta;p)}{\partial\zeta}\dfrac{\partial\Phi(\zeta;p)}{\partial\zeta}+Nt\left(\dfrac{\partial\Theta(\zeta;p)}{\partial\zeta}\right)^2\right)\end{array}\right),$$

(20)

$$N_3\left[F(\zeta;p),\Theta(\zeta;p),\Phi(\zeta;p)\right]=\frac{\partial^2\Phi(\zeta;p)}{\partial\zeta^2}+\frac{Nt}{Nb}\frac{\partial^2\Theta(\zeta;p)}{\partial\zeta^2}$$
$$+\frac{Sc}{m+1}\left(F(\zeta;p)\frac{\partial\Phi(\zeta;p)}{\partial\zeta}-\frac{\partial F(\zeta;p)}{\partial\zeta}\Phi(\zeta;p)-\gamma\Phi(\zeta;p)\right),$$

(21)

where $p\in[0,1]$ is the embedding parameter, $\hbar_1,\hbar_2$ and $\hbar_3$ are non-zero auxiliary parameters and N_1,N_2 and N_3 are nonlinear operators.

The nth-order deformation equations are follows

$$L_1\left(F_n(\zeta)-\chi_n F_{n-1}(\zeta)\right)=\hbar_1 R_n^F(\zeta),$$

(22)

$$L_2\left(\Theta_n(\zeta)-\chi_n \Theta_{n-1}(\zeta)\right)=\hbar_2 R_n^\Theta(\zeta),$$

(23)

$$L_3\left(\Phi_n(\zeta)-\chi_n \Phi_{n-1}(\zeta)\right)=\hbar_3 R_n^\Phi(\zeta),$$

(24)

with the following boundary conditions

$$F_n(0)=0,\quad F_n'(0)=0,\quad F_n'(\infty)=0,$$
$$\Theta_n(0)=0,\quad \Theta_n(\infty)=0,$$
$$\Phi_n(0)=0,\quad \Phi_n(\infty)=0,$$

(25)

where

$$R_n^F(\zeta)=\left(1+\frac{1}{\beta}\right)F_{n-1}'''+\frac{1}{m+1}\left[\sum_{i=0}^{n-1}F_{n-1-i}F_i''-2\sum_{i=0}^{n-1}F_{n-1-i}'F_i'-MF_{n-1}'\right],$$

(26)

$$R_n^\Theta(\zeta)=\left(1+\frac{4}{3}\right)\Theta_{n-1}''+\Pr\left[\begin{array}{l}\dfrac{1}{m+1}\left(\sum_{i=0}^{n-1}F_{n-1-i}\Theta_i'-\sum_{i=0}^{n-1}F_{n-1-i}'\Theta_i+Q\Theta_{n-1}\right)\\ +Nb\sum_{i=0}^{n-1}\Theta_{n-1-i}'\Phi_i'+Nt\sum_{i=0}^{n-1}\Theta_{n-1-i}'\Theta_i'\end{array}\right],$$

(27)

$$R_n^\Phi(\zeta)=\Phi_{n-1}''+\frac{Nt}{Nb}\Theta_{n-1}''+\frac{Sc}{m+1}\left(\sum_{i=0}^{n-1}F_{n-1-i}\Phi_i'-\sum_{i=0}^{n-1}F_{n-1-i}'\Phi_i-\gamma\Phi_{n-1}\right),$$

(28)

$$\chi_n=\begin{cases}0, & n\le 1,\\ 1, & n>1.\end{cases}$$

(29)

Convergence of HAM

The auxiliary parameters $\hbar_1,\hbar_2$ and $\hbar_3$ controls and adjust the convergence of the obtained series solutions. To acquire the apt values for these parameters $\hbar$ - curves are portrayed in Fig. 2. From this figure, the presumable interval of auxiliary parameter is $[-1.4, 0.0]$. The solutions are convergent for whole region of ζ when $\hbar_1=\hbar_2=\hbar_3=-0.65$. Table. 1 shows the convergence of the method.

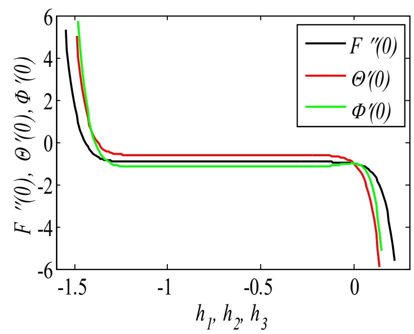

Fig. 2. $\hbar$-curves of $F''(0)\ \Theta'(0)$ and $\Phi'(0)$ for 15th order approximation.

Table 1. Convergence of HAM solutions for different orders of approximations when $\beta=2.0, M=m=0.5, R=0.1, Pr=2.0, Nb=0.3, \chi=Nt=\gamma=Q=0.2, Sc=3.0$

Order	$-f''(0)$	$-\Theta'(0)$	$-\Phi'(0)$
5	0.936668	0.613336	1.177725
10	0.936614	0.613506	1.175343
15	0.936612	0.613362	1.175846
20	0.936612	0.613443	1.175672
25	0.936612	0.613453	1.175740
30	0.936612	0.613463	1.175732
35	0.936612	0.613464	1.175727
40	0.936612	0.613464	1.175727
45	0.936612	0.613464	1.175727

Results and Discussion

The percussion of retained pertinent parameters on the velocity, temperature, concentration, friction factor, local Nusselt number and local Sherwood number are explained.

For numerical solutions we considered the non-dimensional parameter values as $\beta=2.0, M=m=0.5, R=0.1, Pr=2.0, Nb=0.3, \chi=Nt=\gamma=Q=0.2, Sc=3.0$

These values are reserved in entire study apart from the variations in consequent figures and tables.

The resistance force known as Lorentz force is intensified by an expansion in the magnetic parameter, which lowers velocity while rising temperature and concentration in both $\chi=0$ and $\chi \neq 0$. This is delineated in Figs. 3 to 5.

Figs. 6 to 8 show the proclivity of Casson parameter β on the distributions. It is seen that velocity dwindles and temperature and concentration raise with β. This appears due to the increase of plastic dynamic viscosity with β. This is observed in both $\chi=0$ and $\chi \neq 0$.

Fig. 9 to 11 illustrate the impact of velocity index parameter m on velocity, temperature and concentration. These distributions accelerate with m. This is due to the amplification of slenderness in the sheet with m. This is observed in both $\chi=0$ and $\chi \neq 0$.

If the radiation parameter is increased, heat energy is emitted, and as a result, temperature rises with R. The thickness of the thermal boundary layer is much more in $\chi \neq 0$ than $\chi=0$ case. This is represented in Fig. 12.

Temperature decreases and mixed behaviour is observed for concentration profiles due to the slow rate of thermal diffusivity caused by rising Prandtl number Pr. It is observed that thickness of the thermal boundary layer is much bigger in $\chi \neq 0$ case compared to $\chi=0$ case. This is elucidated in Figs. 13 and 14.

Fig. 15 shows the possessions of the Brownian motion parameter Nb on the temperature profiles of the flow. It is observed that with the augmentation in Nb, temperature of the nanofluid enlarges in both $\chi=0$ and $\chi \neq 0$ cases. This may take place since the Brownian motion develops the colloidal fluid particle interaction. Physically when there is higher thickness in the sheet, particle to particle interaction is more. Hence flow over exponentially slendering sheet shows higher temperature profiles compared with exponentially stretching sheet. Fig. 16 describes the weight of Nb on the concentration profiles of nanofluids. Rise in values of Nb shows reduction in nanoparticles diffusion for $\chi=0$ and $\chi \neq 0$ cases.

Figs. 17 and 18 reveal the consequence of thermophoresis parameter Nt on temperature and concentration distributions. Growing values of Nt progress the temperature and concentration profiles for both $\chi=0$ and $\chi \neq 0$ case. Physically due to movement of nanoparticles from hot to cold region with the raise of Nt causes boost in nanoparticle volume fraction and nanoparticle concentration boundary layer thickness.

Due to the production of heat energy in the flow region by the addition of heat source parameter Q temperature lift up with Q. This is given in Fig. 19.

Through Fig. 20, we illustrate the prepotency of Schmidt number Sc on concentration profiles. It is perceptible that an enhancement in Sc depreciates the concentration. This due to the lower molecular diffusivity for the higher values of Sc. Similar effect is observed on concentration profiles for chemical reaction parameter γ also in Fig. 21.

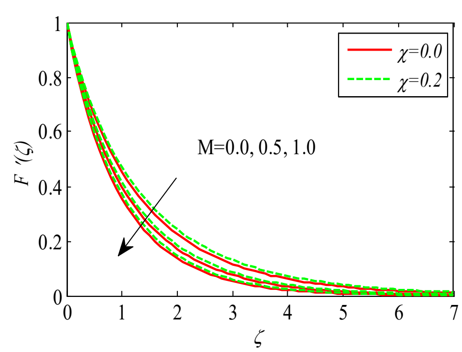

Fig. 3. Effect of M on $F'(\zeta)$.

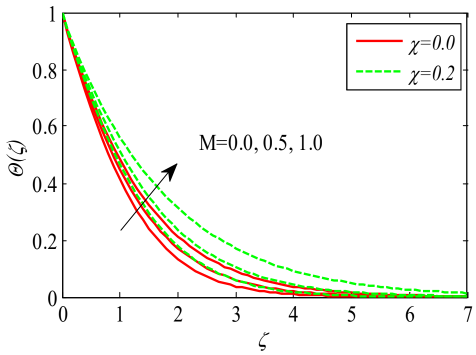

Fig. 4. Effect of M on $\Theta(\zeta)$.

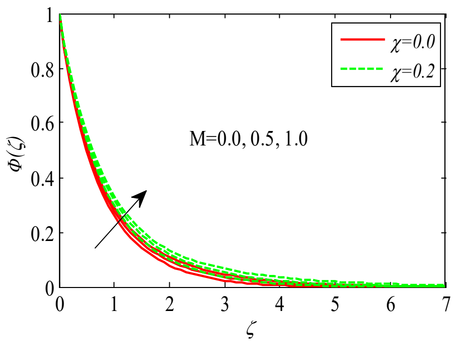

Fig. 5. Effect of M on $\Phi(\zeta)$.

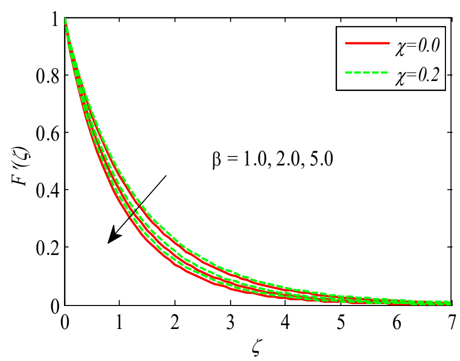

Fig. 6. Effect of β on $F'(\zeta)$.

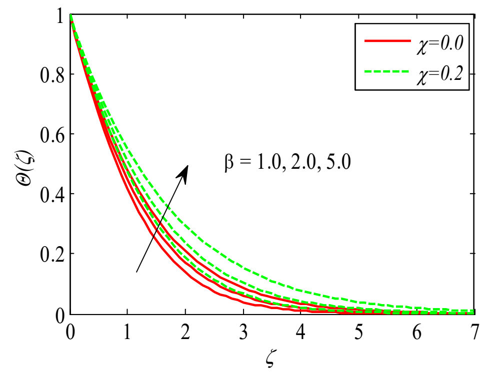

Fig. 7. Effect of β on $\Theta(\zeta)$.

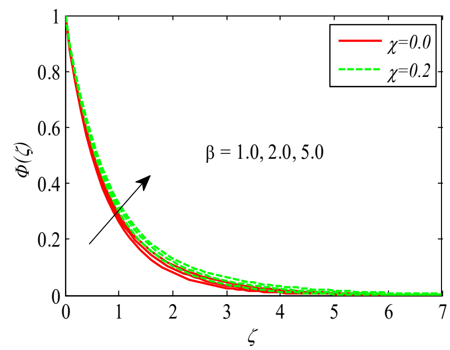

Fig. 8. Effect of β on $\Phi(\zeta)$.

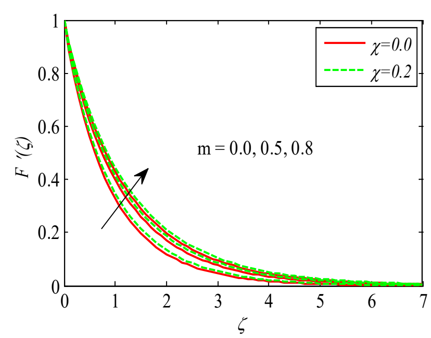

Fig. 9. Effect of m on $F'(\zeta)$.

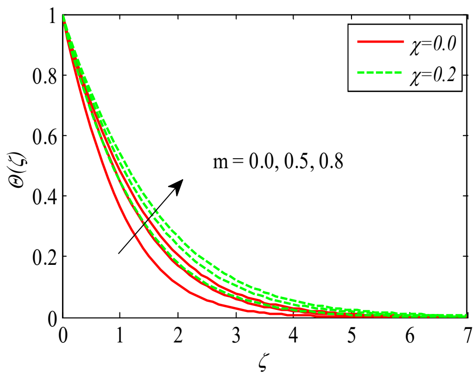

Fig. 10. Effect of m on $\Theta(\zeta)$.

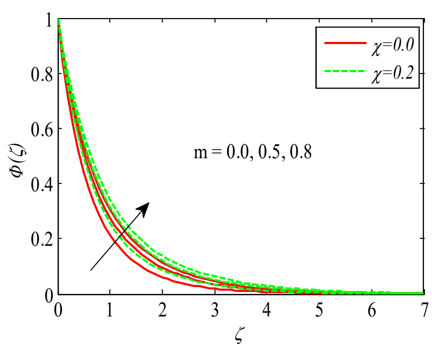

Fig. 11. Effect of m on $\Phi(\zeta)$.

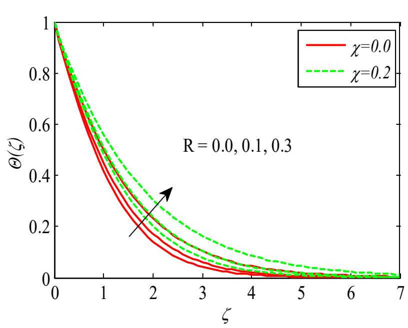

Fig. 12. Effect of R on $\Theta(\zeta)$.

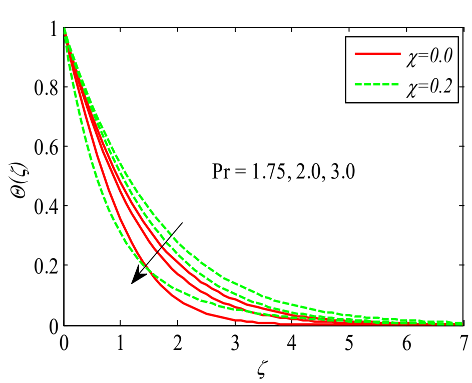

Fig. 13. Effect of Pr on $\Theta(\zeta)$.

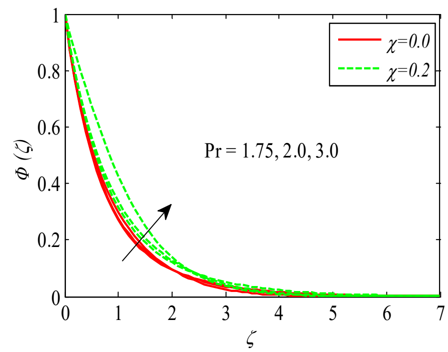

Fig. 14. Effect of Pr on $\Phi(\zeta)$.

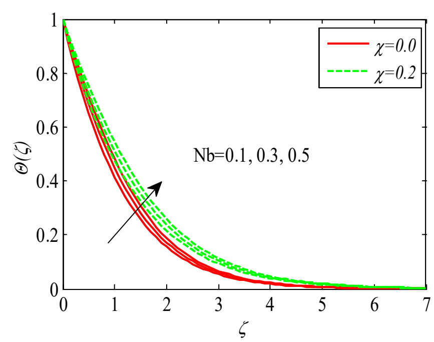

Fig. 15. Effect of Nb on $\Theta(\zeta)$.

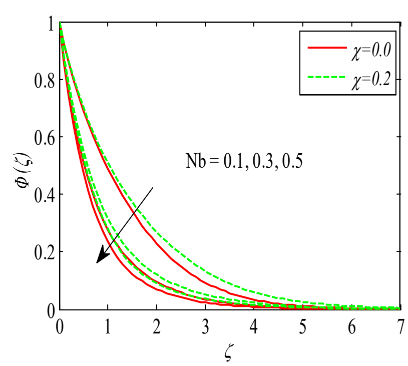

Fig. 16. Effect of Nb on $\Phi(\zeta)$.

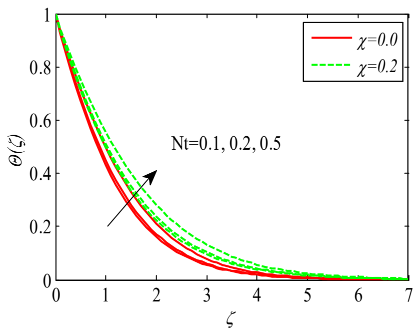

Fig. 17. Effect of Nt on $\Theta(\zeta)$.

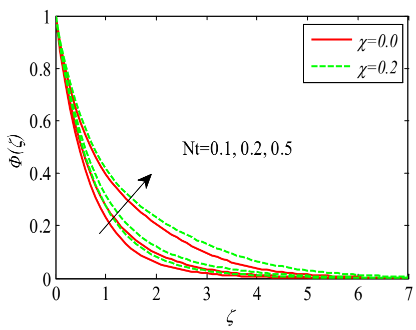

Fig. 18. Effect of Nt on $\Phi(\zeta)$.

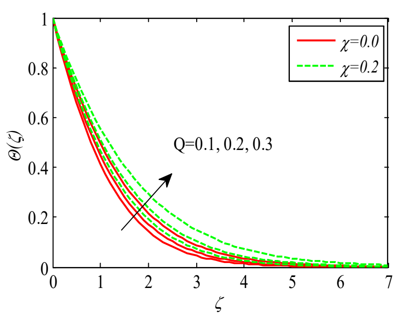

Fig. 19. Effect of Q on $\Theta(\zeta)$.

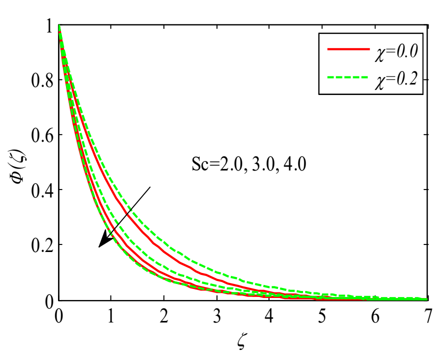

Fig. 20. Effect of Sc on $\Phi(\zeta)$.

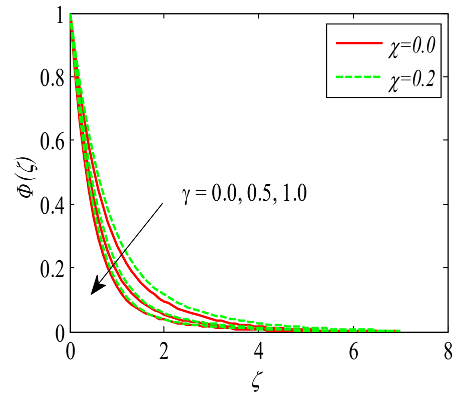

Fig. 21. Effect of γ on $\Phi(\zeta)$.

Impact of M and β on friction factor is shown in Fig. 22. It is seen that C_f decelerates by elevating the values of M and β. Fig. 23, explores the fluctuations of local Nusselt number for various values of Nb and Nt which decreases with the increase of Nb and Nt. From Fig. 24, it is noticed that local Nusselt number decreases with the increase of Q and R. Fig. 25 shows that local Sherwood number decreases by the increase of Pr and Sc.

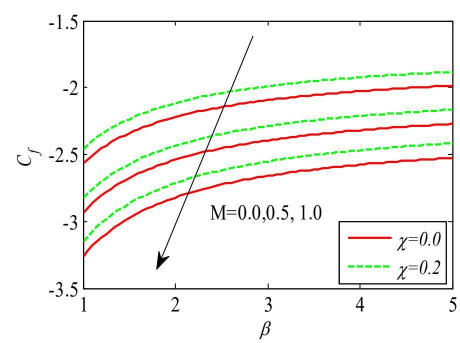

Fig. 22. Effect of M and β on C_f.

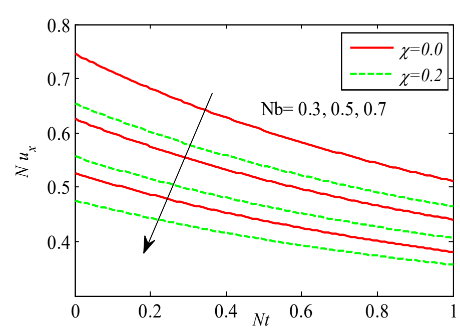

Fig. 23. Effect of Nt and Nb on Nu_x.

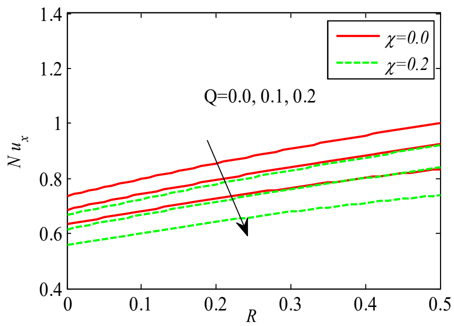

Fig. 24. Effect of Q and R on Nu_x.

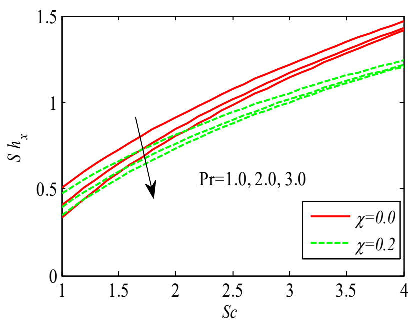

Fig. 25. Effect of Pr and Sc on Sh_x.

In order to verify the accuracy and reliability of the present analysis, the obtained results have been compared with that of Bidin and Nazar [31] and Nadeem et al. [32] solutions for the limiting case when

$$M=0.0,\ \beta\to\infty, m=0.0, \chi=Q=\gamma=0.0, Nb\to 0.0, Nt=0.0$$

. As shown in Table 2, the comparison in the above case is found to be in good agreement.

Table 2. Comparison of $-\Theta'(0)$.

Pr	R	Bidin and Nazar [31]	Nadeem et al. [32]	HAM
1.0	0.0	0.9547	--	0.954784
	0.5	0.6765	0.680	0.676511
	1.0	0.5315	0.534	0.531442
2.0	0.0	1.4714	--	1.471462
	0.5	1.0735	1.073	1.073520
	1.0	0.8627	0.863	0.862771

Conclusions

Here, we analyzed the MHD flow over an exponentially slandering sheet with radiation and heat source. In this procession, we delineated some graphs to describe the pursuance of a few governing parameters on the flow field. The following conclusions have been made through this study.

- Nb and Nt are capable to magnify the temperature of the fluid.
- Enhancement in the velocity power index parameter index parameter exhibits the acceleration in velocity, temperature and concentration profiles.
- Immense thermal boundary layer is noticed in $\chi \neq 0$ when compared with $\chi = 0$.
- Schmidt number and chemical reaction parameter have propensity to decelerate the concentration field.
- There is a perceptible decrease in heat transfer rate with enhancing values of Q and R.

References

1. K.R. Rajagopal, A note on unsteady unidirectional flows of a non-Newtonian fluid, *International Journal of Non-Linear Mechanics,* 17, 369-373, 1982.
2. K.R. Rajagopal, On the creeping flow of the second-order fluid, *Journal of Non-Newtonian Fluid Mechanics,* 15, 239-246, 1984.
3. A.M. Siddiqui and P.N. Kaloni, Certain inverse solutions of a non-Newtonian fluid, *International Journal of Non-Linear Mechanics,* 21, 459-473, 1986.
4. T. Hayat, S. Asghar and A.M. Siddiqui, Some unsteady unidirectional flows of a non-Newtonian fluid, *International Journal of Engineering Science,* 38, 337-346, 2000.
5. D. Vieru, C. Fetecau and C. Fetecau, Exact solutions for the flow of an Oldroyd-B fluid due to an infinite flat plate, *Journal of Applied Mathematics and Physics*, 59, 834-847, 2008.
6. V. Aliakbar, A. Alizadeh-Pahlavan and K. Sadeghy, The influence of thermal radiation on MHD flow of Maxwellian fluids above stretching sheets, *Communications in Nonlinear Science and Numerical Simulation*, 14, 779-794, 2009.
7. T. Hayat and A. H. Kara, Coutte flow of a third-grade fluid with variable magnetic field, *Mathematical and Computer Modelling*, 43, 132-137, 2006.
8. Mahantesh M. Nandeppanavar, K. Vajravelu and M. Subhas Abel, Heat transfer in MHD viscoelastic boundary layer flow over a stretching sheet with thermal radiation and non-uniform heat source/sink, *Communications in Nonlinear Science and Numerical Simulation*, 16, 3578-3590, 2011.
9. B. Sahoo, Flow and heat transfer of a non-Newtonian fluid past a stretching sheet

with partial slip, *Communications in Nonlinear Science and Numerical Simulation*, 15, 602-615, 2010.

10. M. A. A. Hamad, Analytical solution of natural convection flow of a nano fluid over a linearly stretching sheet in the presence of magnetic field, *International Communications in Heat and Mass Transfer*, 38, 487-492, 2011.
11. R. J. Tiwari and M. K. Das, Heat transfer augmentation in two-sided lid-driven differentially heated square cavity utilizing nanofluids, *International Journal of Heat and Mass Transfer*, 50, 2002-2018, 2007.
12. S. E. B. Maiga, S. J. Palm, C. T. Nguyen, G. Roy and N. Galanis, Heat transfer enhancement by using nanofluids in forced convection flows, *International Journal of Heat and Fluid Flow*, 26, 530-546, 2005.
13. M. A. Sheremet, S. Dinarvand and I. Pop, Effect of thermal stratification on free convection in a square porous cavity filled with nanofluid using Tiwari and Das'nanofluid model, *Physica E*, 69, 332-341, 2015.
14. S. Das, R. N. Jana and O. D. Makinde, MHD boundary layer slip flow and heat transfer of nanofluid past a vertical stretching sheet with non-uniform heat generation/absorptyion, *International Journal of Nanoscience*, 13, 1450019, 2014.
15. F. Mabood, W. A. Khan and A. I. M. Ismail, MHD boundary layer flow and heat transfer of nanofluids over a nonlinear stretching sheet : A numerical study, *Journal of Magnetism and Magnetic Materials*, 374, 569-576, 2015.
16. S. A. Shehzad, T. Hayat and A. Alsaedi, Influence of convective heat and mass conditions in MHD flow of nanofluid, *Bulletin of the Polish Academy of Sciences Technical Sciences*, 63, 465-474, 2015.
17. J. V. Ramana Reddy, V. Sugunamma, N. Sandeep and C. Sulochana, Influence of chemical reaction, radiation and rotation on MHD nanofluid flow past a permeable flat plate in porous medium, *Journal of the Nigerian Mathematical Society*, 35, 48-65, 2016.
18. Swati Mukhopadhyay, Casson fluid flow and heat transfer over a nonlinear surface, *Chinese Physics B*, 22, 074701, 2013.
19. S. Pramanik, Casson fluid flow and heat transfer past an exponentially porous stretching surface in presence of thermal radiation, *Ain Shams Engineering Journal*, 5, 205-212, 2014.
20. S. Nadeem, Rizwan Ul Haq, Noreen Sher Akbar and Z. H. Khan, MHD three-dimensional Casson fluid past a porous linearly stretching sheet, *Alexandria Engineering Journal*, 52, 577-582, 2013.
21. S. M. Ibrahim, G. Lorenzini, P. Vijaya Kumar and C. S. K. Raju, Influence of chemical reaction and heat source on dissipative MHD mixed convection flow of a Casson nanofluid over a nonlinear permeable stretching sheet, *International Journal of Heat and Mass Transfer*, 111, 346-355, 2017.
22. S. M. Ibrahim, P. V. Kumar, G. Lorenzini, E. Lorenzini and F. Mabood, Numerical study of the onset of chemical reaction and heat source on dissipative mhd stagnation point flow of Casson nanofluid over a nonlinear stretching sheet with velocity slip and convective boundary conditions, *Journal of Engineering Thermophysics*, 26, 256-271, 2017.
23. L. Lee, Boundary layer over a thin needle, *Physics of* Fluids, 10, 820-822, 1967.
24. T. Fang, J. Zhang and Y. Zhong, Boundary layer flow over a stretching sheet with variable thickness, *Applied Mathematics and Comutations*, 218, 7142-7252, 2012.
25. M. M. Khader and Ahmed M. Megahed, Numerical solution for boundary layer flow due to a nonlinearly stretching sheet with variable thickness and slip velocity, *The European Physical Journal Plus*, 128, 100-108, 2013.
26. M. M. Khader and Ahmed M. Megahed, Boundary layer flow due to a stretching sheet with a variable thickness and slip velocity, *Journal of Applied Mechanics and Technical Physics*, 56, 241-247, 2015.
27. S. J. Liao, Homotopy analysis method in nonlinear differential equations, *Springer & Higher Education Press*, Heidelberg, 2012.
28. T. Hayat, S. A. Shehzad and A. Alsaedi, Soret and Dufour effects on Magnetohydrodynamic (MHD) flow of Casson fluid, *Applied Mathematics and Mechanics*, 33, 1301-1312, 2012.
29. S. M. Ibrahim, P. V. Kumar and G. Lorenzini, Analytical modeling of heat and mass transfer of radiative MHD Casson fluid over an exponentially permeable stretching sheet with chemical reaction, *Journal of Engineering Thermophysics*, 29, 1, 136-155, 2020.
30. Prathi Vijaya Kumar, Shaik Mohammed Ibrahim and Kanithi Jyothsna, Numrical Modeling on radiative dissipative MHD flow of a chemically Casson fluid over an

exponentially inclined stretching sheet, *Mathematical Modelling of Engineering Problems*, 6, 4, 491-501, 2019.

31. B. Bidin and R. Nazar, Numerical solution of the boundary layer flow over an exponentially stretching sheet with thermal radiation, *European Journal of Scientific Research*, 33, 710-717, 2009.
32. S. Nadeem, S. Zaheer and T. Fang, Effects of thermal radiation on the boundary layer flow of a Jeffrey fluid over an exponentially stretching surface, *Numerical Algorithms*, 57, 187-205, 2011.